N88-11145

THE FOUR SPOT TIME-OF-FLIGHT LASER ANEMOMETER

Mark P. Wernet
NASA Lewis Research Center
Cleveland, Ohio

INTRODUCTION

A new time-of-fight laser anemometer system utilizing a spatial lead-lag filter for bipolar pulse generation has been constructed, and initial testing has been initiated. This new TOF has been modified to enable measurements high velocity, turbulent gas flows near walls. Good results have been obtained to 75 μm normal to the surface, with an F number 2.5 collecting lens. Further testing of the new system will be conducted in open jet burner facility in CE-13 to evaluate its suitability for use in hot section flow experiments.

A laser anemometer offers a nonintrusive method for obtaining flow-field information. Particles entrained in the flow provide scattering centers for the incident light. Two common techniques for optically coding the measurement region exist. The laser fringe anemometer (LFA) employs a sinusoidally varying fringe pattern. Knowledge of the fringe spacing and the detected frequency of particles traversing the measurement region permits the determination of the velocity component normal to the fringes. Another technique for encoding the measurement region uses two closely spaced spots, where the flow velocity component parallel to the axis of the spots is obtained from the time-of-flight of particles traversing the two spots.

The motivation for this work was the desire for an anemometer capable of measurements near walls in turbulent flows. This requires a laser anemometer with special qualities. The optimum anemometer would have a wide acceptance angle, to enable measurements of wide flow angle variations, and also have a high spatial selectivity, to limit unwanted flare light scattered from surfaces from reaching the detector. The LFA typically has a wider acceptance angle than a conventional time-of-flight (TOF) system (ref. 1). The lower acceptance angle reduces the utility of TOF systems in turbulent flows. However, the TOF receiver can have much better spatial resolution than the LFA for the same f/number system.

In this work we describe a new, modified TOF system that has been constructed and tested for turbulent flow measurements near walls. The new TOF system uses elliptical spots to increase the flow acceptance angle to be comparable with that of an LFA. Also, the new TOF uses an optical code that vastly simplifies the pulse-detection processor. A simple electronic pulse position technique was used instead of the more complex correlation techniques (refs. 2 to 4).

THEORY

The electronic signal obtained from a normal two-spot TOF system consists of two noisy gaussian shaped pulses separated by the transit time of a particle traversing the two light spots in the measurement region. An estimate of the peak to peak time of flight and knowledge of the spot spacing then yields the particle velocity component along the axis of the two spots. The inherent noise on any type of photon-

detection system decreases the ability of the signal processor to determine the exact time-of-occurrence of a pulse. The particle's time of flight can be obtained more accurately by transforming the unipolar pulse into a bipolar pulse. The zero crossings of the bipolar pulses yield the estimated time of flight. The transformation from a unipolar to a bipolar pulse should not introduce additional noise to the signal. Lading (ref. 1) analyzed the performance of three methods for generating bipolar pulses: the derivative operator, Hilbert transforms, and the spatial lead-lag filter. He found that the Hilbert transform and spatial lead-lag filters were less sensitive to the signal bandwith. The derivative operator yielded optimum performance when the filter bandwith was equal to the signal bandwith. He suggested that an advantage could be obtained by implementing the lead-lag filter spatially, before photon detection. The advantage of the spatial lead-lag filter is that the dimensions are fixed in space, but the temporal scale of the signal depends on the velocity. Thus, a spatial implementation will behave as an adaptive temporal lead-lag operator. The transformation to a bipolar pulse is thus made without adding noise to the signal and in a robust manner that does not depend on electronic delays. The TOF system described herein has a spatial lead-lag filter.

IMPLEMENTATION

The new TOF system uses two pairs of elliptical spots in the measurement region. These two pairs of spots, labeled A to D, are separated by a distance X_0 and orthogonally polarized and partially overlapping (fig. 1). The use of elliptical spots increases the acceptance angle of the measurement region, comparable with that of a laser fringe anemometer.

The transmitting section of the system contains two quarter-wave plate/Wollaston prism pairs (fig. 2). The input light is linearly polarized. A cylindrical lens transforms the circular input beam into an elliptical beam. The first quarter-wave plate/Wollaston prism pair Q_1/W_1 generates two angularly diverging, orthogonally polarized beams. These plane, polarized beams are imaged by L_2 and L_3 onto the second pair Q_2/W_2. The first pair Q_1/W_1 must be at the back focal plane of L_2, and Q_2/W_2 must be at the front focal plane of L_3 to maintain the sharpness of the imaged spots. Emerging from the Q_2/W_2 pair are four consecutively, orthogonally polarized beams. The angular divergence of these beams is transformed into a spatial separation by the lens L_4. The angular divergence imparted by the Q_1/W_1 pair creates the spatial separation X_0. The angular divergence imparted by Q_2/W_2 creates the partially overlapping spots in the measurement region.

The measurement region geometry is controlled by the input beam diameter, by the angular divergences of W_1 and W_2, and by the focal length of L_4. The position of L_4 is the most critical adjustment in the transmitter. A very smooth, linear positioning translator is required to position L_4 such that the Q_2/W_2 pair is at the back focal plane. This critical adjustment determines the sharpness of the spots at the focal plane and their relative separation. To generate pulses of roughly equal amplitude, the quarter-wave plate/Wollaston prism pairs will each have to be adjusted to equalize the intensities of the four spots.

The backscatter system configuration collects the scattered light from the measurement region back along the axis of the transmitted beam. The use of the two elevation mirrors M_1 and M_2 allows this coaxial configuration. The received image is magnified by the image pair L_4 and L_7. The rectangular mirror M_2 acts as a vertical spatial filter mask in the receiver. The received light is recombined into two pairs of totally overlapping spots by a third Wollaston prism,

W_3 which has the same angular split as W_2. These two spots are imaged onto the receiver mask consisting of two precision air slits. The two totally overlapping pairs of spots are separated by a polarization-selective beam-splitting cube. Two right-angle prisms are used to separate the spot pairs into four individual signals. The separated signals are detected by four RCA 8645 photomultiplier tubes.

The receiver system shares the image pair L_5 and L_6 with the transmitter. Lenses L5 and L6 are 100 mm in diameter and have focal lengths of 500 and 250 mm, respectively. The receiver system is sensitive to the position of lens L_4. The use of L_4 as a common lens focuses both the transmitter and receiver simultaneously. No extensive amount of flare light has been observed from this configuration.

A dove prism image rotator has been incorporated into the new TOF system. The image rotator is common to both the transmitter and receiver. The image rotator permits two-dimensional velocity scans by taking measurements at several angular orientations of the measurement volume.

A prototype system has bee constructed and tested in cooperation with Dr. R.V. Edwards at Case Western Reserve University. The second-generation system has been constructed at Lewis from optical erector components (figs. 3 and 4). An argon-ion laser source, operating at 300 mW and 514.5 nm, was used. The specifications of the critical optical components used are

$$W_1 = 5 \text{ mrad}$$

$$W_2 = W_3 = 250 \text{ μrad}$$

$$L_4 = 80 \text{ mm}$$

The resulting measurement region geometry was

Elliptical spot width, μm	20
Elliptical spot height, μm	280
Spot overlap, μm	12
Spot pair spacing, μm	200
Acceptance angle,	+/-50°

OPERATION

The temporal separation of the bipolar pulses is detected by a zero crossing detection circuit. Figure 5 shows the signal processing electronics. There are six input signals to the pulse detection circuit: the A, D, A + B, A - B, C + D, and C - D signals. The circuit uses the A and D signals to determine the direction of the detected particle. The A + B and C + D signals are used to enable comparators to search for the zero crossings of the A - B and C - D signals, respectively. The amplitude where either the A + B or the C + D signal enables the comparator is the threshold level. A particle traversing from the left, through the AB and then CD spot pairs yields an A + B signal, which enables the A + B comparator. The circuit finds the A - B zero crossing and then disables the A + B comparator until either the particle is detected at C + D or the time window expires. The time window is set as the maximum time the processor will wait for a signal from the CD spot pair, that is, the slowest expected velocity, before resetting the circuit. The analogous process occurs for a particle traversing from the opposite direction, first enabling C + D. The circuit now searches for the C - D

zero crossing and then disables the C + D comparator until either a particle is detected at A + B or, again, until the time window expires. This technique yields the flow direction and minimizes the number of false counts due to simultaneous particles in the measurement region and/or particles traversing only one of the spot pairs.

The zero crossing detection circuit outputs start and stop pulses, which are fed into a time analyzer. The start and stop pulses correspond to a particle traversing the two pairs of spots in the measurement region, that is, the time of flight. The time analyzer generates a voltage pulse (0 to 10 V) that is proportional in amplitude to the time difference between the start-stop pulses. These voltage pulses are sent to a pulse height analyzer, which sorts the voltage pulses and makes a histogram of their amplitude. The pulse-height analyzer uses 1024 bins to display the time-of-flight probability distribution (TPD) on an internal cathode ray tube (CRT). The TPD's were transferred to a personal computer, via an RS-232 interface, for analysis. The future data acquisition system will use the time analyzer output and an analog to digital converter to convert the time-of-flight into digital words. The digital data will be sent to a TSI Model 1998 master interface and then to a PDP 11/44 computer for analysis.

EXPERIMENT

The ability to discriminate against light not originating at the focii of the TOF beams is a very important characteristic of a practical laser anemometer. Particles traveling at a different velocity than particles at the focal plane, that is when a velocity gradient exists across the measurement volume, may scatter light which is detected by the system. Thus a spread of velocities will be measured. One wishes to minimize this spread. Shot noise from light scattered from walls decreases the signal-to-noise ratio and requires a higher threshold level for optimum signal processing. Hence, this shot noise caused from flare light is the limiting factor in how close to a wall one can get and obtain a measurement of the flow velocity.

A practical test of an anemometer's spatial selectivity is obtained by operating the system in a flow near a wall. A boundary-layer flow field would supply the necessary measurement environment. The boundary-layer thickness $\delta(x)$ was defined as the distance from the surface where the velocity reached 99 percent of the free-stream velocity. Two experimental setups were used. A rectangular nozzle (6 by 12 mm) with an access window provided an environment similar to that encountered in a windowed engine casing. Measurements were made in the boundary layer that formed off the back wall of the nozzle. The back wall was painted black to reduce the amount of flare light. The second setup consisted of a low-velocity circular nozzle. A flat plate was placed parallel to the flow at the nozzle exit and perpendicular to the incoming light. The flat plate had a smooth polished surface. These two setups yielded a measure of how close to a wall measurements can be obtained.

The time probability distributions were converted to velocity probability distributions (VPD) using the known spot spacing. The velocity distributions were measured at various points along a line perpendicular to the plane of the surface. The variance of the VPD gives an estimate of the range of velocities present across the length of the sample volume. The mean velocities at each measurement position were fit to a cubic polynomial describing the boundary-layer velocity profile. The variances of the VPD's were plotted versus distance from the surface.

The results of these boundary-layer profiles are shown in figures 6 to 9. Figure 6 shows the mean velocity versus distance from the surface for the windowed nozzle flow. Measurements were obtained to 100 μm from the surface for this setup. Figure 7 shows the velocity variance versus position for the profile of figure 6. The threshold level in the signal processor was adjusted at each measurement position to minimize the background noise. This accounts for the variation in the measured velocity variances in this figure.

Figures 8 and 9 show the mean velocity and velocity variance versus position for the flat-plate configuration, respectively. The profile was made 1 cm from the leading edge of the plate. Measurements were obtained 75 μm from the surface of the plate. The threshold level was held constant for the entire profile. Figure 9 shows the expected behavior of increasing velocity variance inside the boundary layer as the magnitude of the velocity gradient increases.

The contraction nozzles used to supply the flow fields were driven by the building service air. The low-velocity limit restricts the pressure drop across the nozzle to approximately 0.1 psia. Fluctuations in the service air cause perturbations in the flow field. Some of the structures observed in these boundary-layer profiles may be artifacts of the service air fluctuations.

This second-generation four-spot TOF system uses a new prototype zero crossing detection circuit. The prototype signal processor uses the more robust processing scheme described above. The upper bandwidth limit on the prototype signal processor limits the maximum measurable velocity at approximately 40 m/sec. A new high-speed ECL version is under construction.

CONCLUSIONS

The newly constructed, four-spot anemometer has been shown to perform as predicted. The new anemometer's measurement region has the required characteristics: wide acceptance angle and high spatial selectivity to permit measurements in turbulent, hostile environments.

REFERENCES

1. L. Lading; "Estimating Time and Time Lag in Time-of-Flight Velocimetry," Appl. Opt. 22, 3637-3643, 1983.

2. M.J. Fisher and F.R. Krause; The Crossed-Beam Correlation Technique, J. Fluid Mech. 28, 705-717, 1967.

3. W. Matthes, W. Riebold, and E. de Cooman; Measurement of Gas Bubbles in Water by a Correlation Method, Rev. Sci. Instr. 41, 843-845, 1970.

4. T.S. Durrani and C.A. Greated; Spectral Analysis and Cross-Correlation Techniques for Photon Counting Measurements in Fluid Flows, Appl. Opt. 14, 778-786, 1975.

5. L. Lading; Comparing a Laser Doppler Anemometer with a Laser Correlation Anemometer, "Conference on the Engineering Uses of Coherent Optics," Glasgow, 493-510, Cambridge University Press, 1975.

FOUR-SPOT ANEMOMETER MEASUREMENT VOLUME GEOMETRY

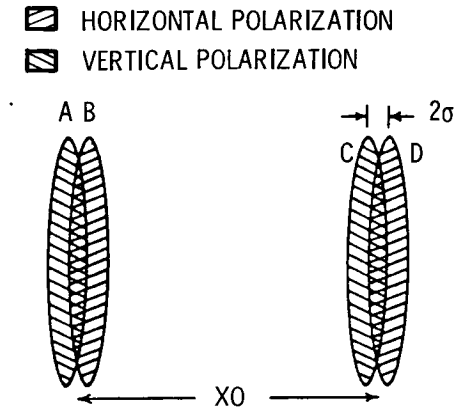

CS-85-3324

Figure 1

FOUR-SPOT ANEMOMETER OPTICAL COMPONENT LAYOUT

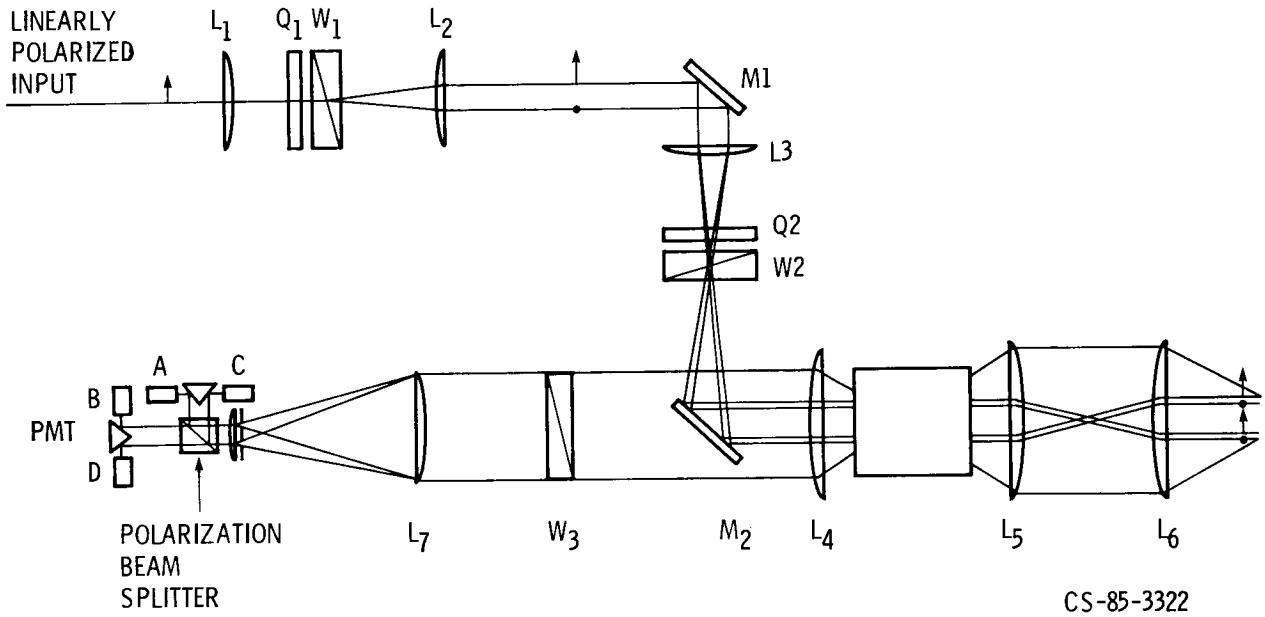

CS-85-3322

Figure 2

FOUR-SPOT ANEMOMETER CONSTRUCTED FROM OPTICAL ERECTOR COMPONENTS

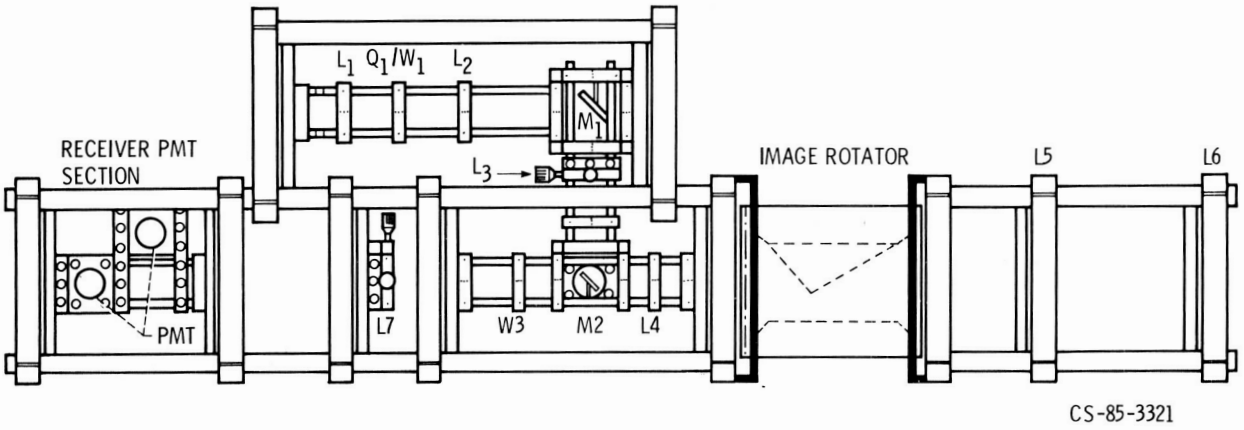

Figure 3

FOUR-SPOT ANEMOMETER PHOTOGRAPH

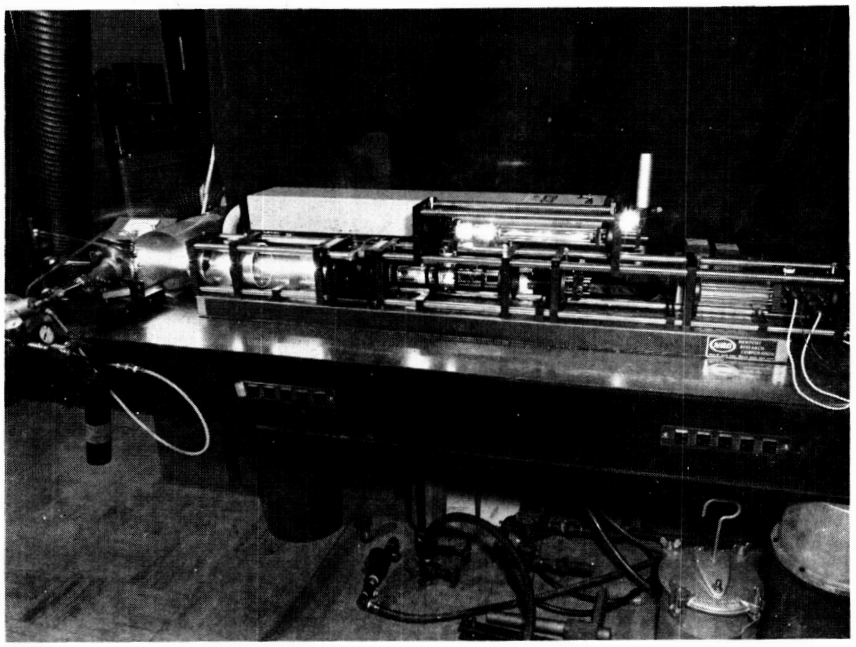

Figure 4

SIGNAL PROCESSING FLOW CHART

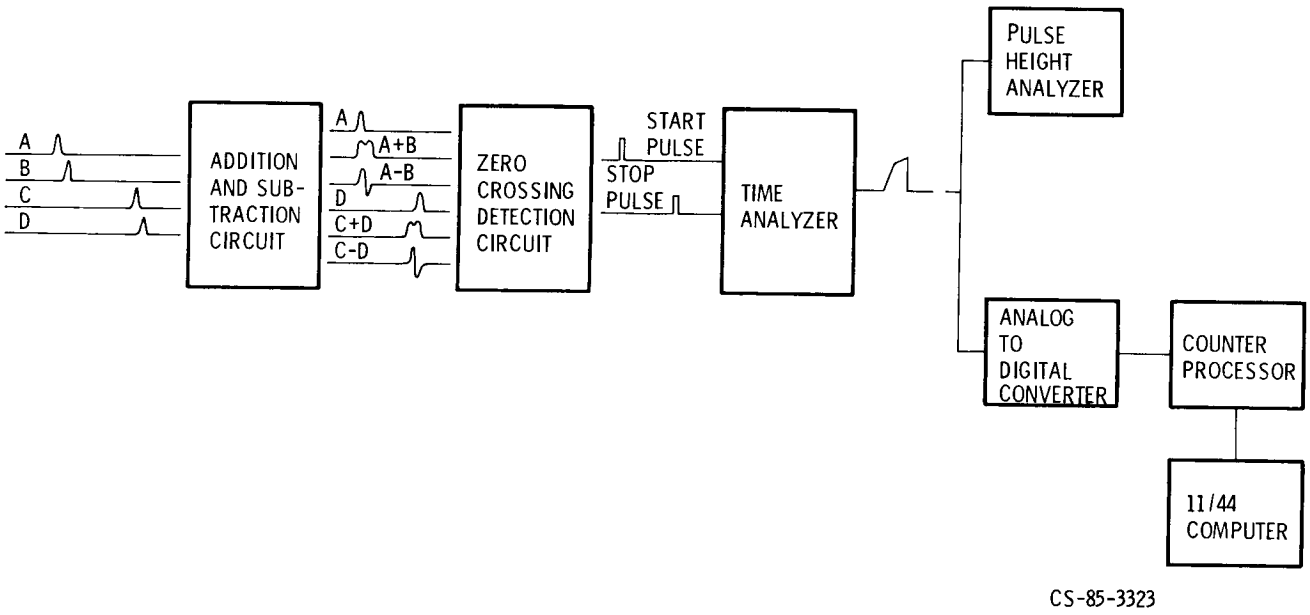

Figure 5

WINDOWED NOZZLE BOUNDARY LAYER FLOW

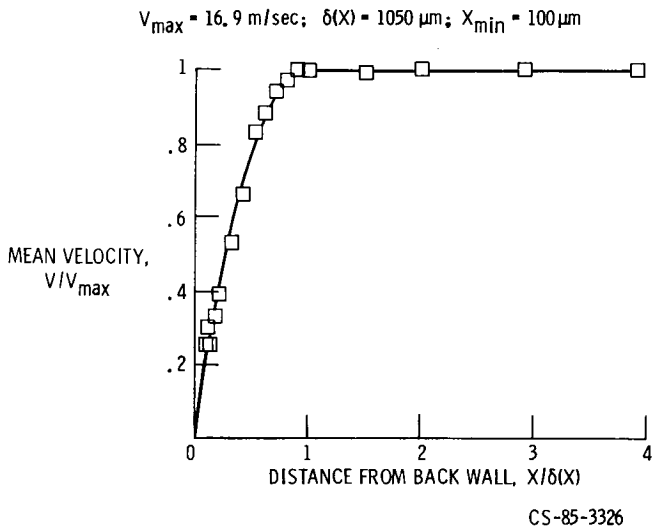

Figure 6

VELOCITY VARIANCE VS POSITION FOR WINDOWED NOZZLE BOUNDARY LAYER FLOW

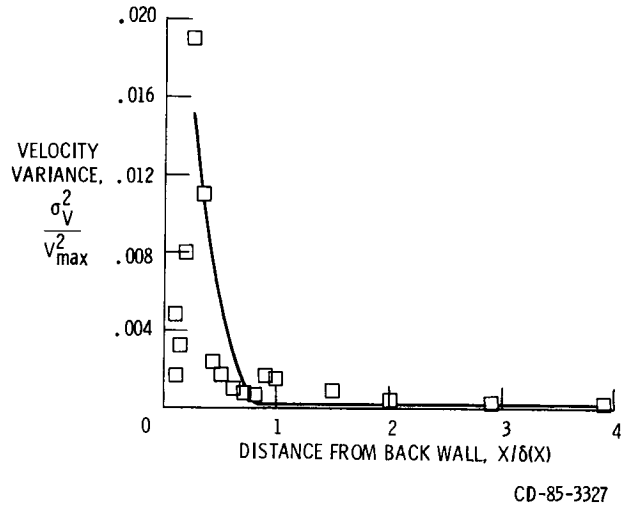

Figure 7

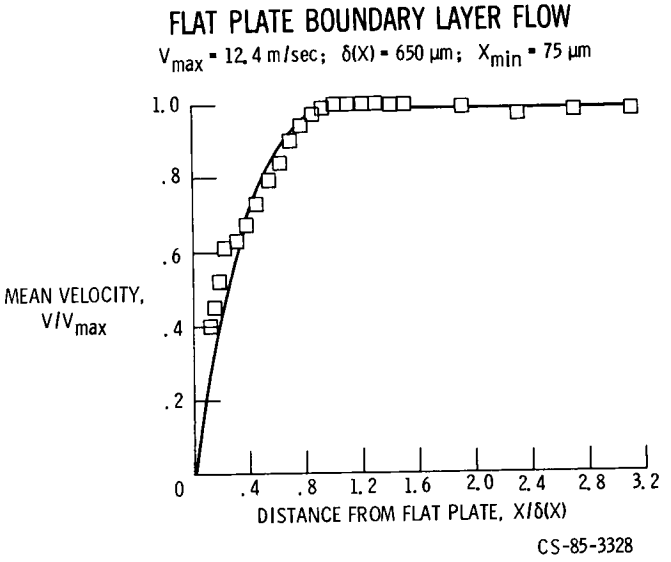

Figure 8

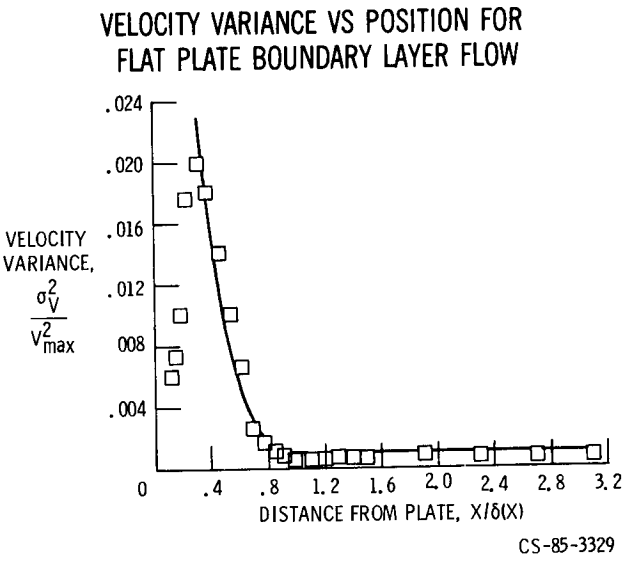

Figure 9